Title

β-Diketonate-Iron(III) Complex: A Versatile Fluorine-19 MRI Signal Enhancement Agent

Journal

ACS Applied Bio Materials, 2(9)

ISSN

2576-6422

Authors

Wang, Chao
Adams, Stephen R
Xu, Hongyan
et al.

Publication Date

2019-09-16

DOI

10.1021/acsabm.9b00455

Peer reviewed

HHS Public Access

Author manuscript

ACS Appl Bio Mater. Author manuscript; available in PMC 2021 May 11.

Published in final edited form as:

ACS Appl Bio Mater. 2019 September 16; 2(9): 3836–3842. doi:10.1021/acsabm.9b00455.

β–Diketonate-Iron(III) Complex: A Versatile Fluorine-19 MRI Signal Enhancement Agent

Chao Wang[†], **Stephen R. Adams**[‡], **Hongyan Xu**[†], **Wenlian Zhu**[†], **Eric T. Ahrens**[*,†]

[†]Department of Radiology, University of California, San Diego, La Jolla, California 92093, United States

[‡]Department of Pharmacology, University of California, San Diego, La Jolla, California 92093, United States

Abstract

Fluorine-19 magnetic resonance imaging (MRI) has gained considerable momentum as a promising imaging modality for in vivo tracking of cellular therapies and as a diagnostic for inflammatory disease. To further the utility of this technique, we increase imaging probe sensitivity by merging paramagnetic metal chelates with aqueous perfluorocarbon (PFC) nanoemulsions. We prepared a highly fluorinated ferric tris(β-diketonate) chelate (MW = 1265.2 g/mol) at gram scale. This iron chelate is soluble in multiple PFC oils used for MRI and readily reduces the ^{19}F longitudinal relaxation time (T_1) to <100 ms with modest line broadening and displays superior properties for ^{19}F MRI applications. The sensitivity enhancement by Fe(III) laden PFC nanoemulsion was confirmed in MRI phantom studies, where reduced T_1 speeds data acquisition thereby increasing the ^{19}F image sensitivity per time via signal averaging. Additionally, ^{19}F relaxivity of nanoemulsions incorporating other metal ions, including Gd, Er, Ho, Dy, Mn, Cr, and Ni, were evaluated. High-moment lanthanide ions, such as Gd(III), display severe line broadening, but other ions [e.g., Ho(III)] induce pseudocontact chemical shifts (up to 0.5 ppm) of ^{19}F in nanoemulsion, which makes them potentially useful for multichromatic ^{19}F imaging. Formulated nanoemulsions have a shelf life >200 days. Free β-diketonate or its iron complex in formed PFC nanoemulsion did not induce cytotoxicity in intracellularly labeled macrophages. Overall, ferric tris(β-diketonate) chelate provides a scalable approach for boosting sensitivity of PFC-based ^{19}F MRI probes. More generally, it can functionalize PFC oil, whose chemical modification remains challenging.

Graphical Abstract

[*]**Corresponding Author:** eta@ucsd.edu. Phone: (858) 246-0279 (E.T.A.).

ASSOCIATED CONTENT

Supporting Information

The Supporting Information is available free of charge on the ACS Publications website at DOI: 10.1021/acsabm.9b00455.

Additional materials and methods associated with synthesis, characterization of compounds, emulsification methods, measurements of relaxivity and solubility, biological cell studies, and crystallization methods (PDF)

Crystallographic information file for $C_{30}H_{12}F_{39}FeO_6$ (CIF)

The authors declare the following competing financial interest(s): E.T.A. is founder, consultant, member of the advisory board, and shareholder of Celsense, Inc.

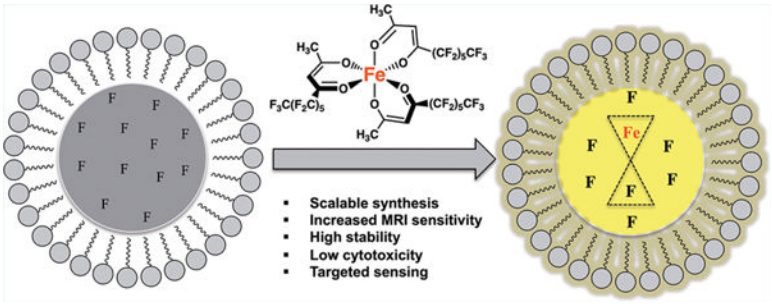

Keywords

MRI; ^{19}F; metal chelate; perfluorocarbon; nanoemulsion; macrophage; inflammation

1. INTRODUCTION

In the past decade, cell therapy trials have experienced tremendous growth, particularly in in the field of immuno-oncology.[1–4] Innovation in imaging methods is urgently needed to elucidate the fundamental behaviors of injected cell therapies in vivo, including their homing sites, survival, and migration pathways.[5–7] Additionally, new diagnostic imaging biomarkers are needed to visualize and quantify sites of cellular inflammation to identify and monitor disease progression as well as the tumor microenvironment.

Optical-based cell imaging has been widely used for in vivo imaging via chemical tagging of cells or by using reporter genes. However, these approaches have severe tissue depth penetration limitations for detection[8,9] and are often not suitable for clinical trial use. The use of radioactive tracers such as ^{111}In, ^{64}Cu, or ^{18}F has also been exploited for nuclear imaging of cell grafts, but challenges remain regarding potential cytotoxicity, image specificity, and long-term cell detection.[10,11]

Magnetic resonance imaging (MRI) is also an option to visualize cell therapies and inflammation in vivo.[12–14] Recent interest has focused on using perfluorcarbon (PFC) based nanoemulsion (NE) probes to intracellularly tag cells which are then detected by fluorine-19 MRI. Output images display “hot spots” at sites of cell accumulation in the body without background[15–19] because of the sparsity of fluorine atoms in wild-type tissues (<1 nmol/g wet tissue).[20,21]

A challenge in the design of suitable fluorine-based agents is maximizing ^{19}F MRI sensitivity. Formulation of ^{19}F-dense PFC oil as a colloidal NE is key to increasing the fluorine cargo endocytosed by cells.[22] To further amplify the NE sensitivity, one can reduce the intrinsically high longitudinal relaxation time (T_1) of PFC, typically ranging from 0.5 to 3 s, that can limit the achievable signal-to-noise ratio (SNR) in a given MRI scan time when repetitive signal averaging is employed.[23] An effective strategy to shorten T_1 is using fluorophilic paramagnetic metal chelates that reduce the relaxation time of ^{19}F via intermolecular, electron–nuclear dipolar interactions, which scales with the metal–fluorine

distance to the negative sixth power.[24] This approach is preferable compared to tethering the paramagnetic agent to the NE surface yielding a larger average metal–fluorine distance.

Recently, Kislukhin et al.[25] and Jahromi et al.[26] described synthetic strategies for the production of fluorophilic metal chelates. In both studies, Fe(III) was observed to be the optimal metal additive to achieve the minimum ratio of T_1 to transverse relaxation time (T_2) of fluorine atoms. In the first approach ("FETRIS"),[25] metal-binding β-diketones were conjugated to end groups of a linear perfluoropolyether (PFPE, M_n = 1750 g/mol). Conjugate oil was blended with unconjugated PFPE, formulated into aqueous NE, and metalated by addition of metal ions to the aqueous phase which is sequestered to fluorous-phase chelate. The Jahromi et al.[26] study described synthesis of a smaller chelate (MW = 1436 g/mol) based on a fluorinated hexadentate imine compound named SALTAME. Chelate is metalated prior to blending with PFC oil followed by NE formulation. Overall, SALTAME requires laborious purification of several isomers, with a single isomer showing satisfactory stability only in perfluorooctyl bromide (PFOB).

Building on these results, we describe the use of a commercially available (perfluoroheptanoyl)acetone (PFHA) precursor for the facile preparation of a new ferric tris(β-diketonate) complex, yielding Fe-PFHA in multigram scale, thereby greatly streamlining paramagnetic NE synthesis. The Fe-PFHA is soluble in a wide range of PFCs of various polarities and effectively enhances the ^{19}F relaxation rates, especially T_1. We studied the performance of Fe-PFHA in perfluoro-15-crown-5-ether (PFCE) NE in detail. PFCE has 20 equiv. of fluorine atoms providing high ^{19}F MRI sensitivity. In addition to iron, we evaluated the ^{19}F relaxivity of other paramagnetic ions, including Gd, Er, Ho, Dy, Mn, Cr, and Ni in PFCE NE. The relaxivity is measured by titrating metal salts to PFC NEs and recording the ^{19}F relaxation times, T_1 and T_2, with different metal concentrations in PFC oil; the slope of the resulting curve yields the relaxivity in units of $mM^{-1}\ s^{-1}$ and is denoted r_1 and r_2, respectively. We performed in vitro macrophage cell labeling studies using NE containing PFHA or Fe-PFHA to elucidate cell uptake and viability at varying doses. Phantom ^{19}F MRI samples containing Fe-PFHA NE display predictable SNR enhancement compared to iron-free NE. Overall, Fe-PFHA has desirable properties for^{19}F MRI applications, and this new synthesis path will accelerate the use of paramagnetic NE in imaging studies.

2. MATERIALS AND METHODS

2.1. Materials.

Chemicals were purchased from Sigma-Aldrich (St. Louis, MO) and solvents were purchased from Fisher Scientific (Pittsburgh, PA) and used without further purification. Fluorous solvents were purchased from Exfluor Research Corporation (Round Rock, TX). The (perfluoroheptanoyl)acetone (PFHA) was purchased from SynQuest laboratories (Alachua, FL).

2.2. Analytic Methods.

Elemental analysis (Table S1), including inductively coupled plasma mass spectrometry (ICP-MS, NEXION 350D, PerkinElmer, Waltham, MA), CHN analysis (CE 440, Exeter Analytical, Chelmsford, MA), and halide analysis (Orion Ion Selective Electrodes, Thermo Fisher Scientific, Waltham, MA), was performed by the Microanalysis Laboratory, University of Illinois at Urbana–Champaign. High-resolution mass spectrometry (HRMS) was performed by the Molecular Mass Spectrometry Facility at the University of California San Diego. Ultraviolet–visible (UV–vis) absorption spectra were recorded on a Shimadzu UV-2700 (Kyoto, Japan) spectrophotometer. Nanoemulsion size and polydispersity was measured using a dynamic light scattering (DLS) instrument (Malvern Zetasizer ZS, Malvern, PA).

2.3. NMR Measurements.

NMR spectra, relaxation times, and microimaging MRI data were recorded on a Bruker 400 MHz (9.4 T) spectrometer (Bruker BioSpin, Billerica, MA) using methods described elsewhere.[26] In PFCs, the major peaks in ^{19}F NMR are used to calculate relaxation times. For PFOB, the −83 ppm ^{19}F, proximal to bromine atom, is used to calculate relaxation times. To measure the nanoemulsion uptake in RAW264.7 cells, an aliquot of 3 million cells were pelleted and suspended in 0.1 mL of lysis buffer (20 mM Tris-HCl, 100 mM NaCl, 1 mM EDTA, 0.5% Triton X-100), followed by the addition of 0.1 mL NaTFA (10 mM in H_2O/D_2O = 9/1) as an internal standard. The ratio of PFC to NaTFA peak integrals were used to determine the amount of ^{19}F in the cell pellet.

2.4. Phantom MRI.

Phantom MRI samples were made using 10 mm NMR tubes, each containing two 3 mm NMR tubes containing PFCE and PFCE-Fe-PFHA ([Fe-PFHA] = 30 mM in PFCE oil) nanoemulsions mixed with 2% agarose in 1:1 (v/v) ratio. The agarose is added to hinder settling of the dense NE during the data acquisitions to ensure uniform ^{19}F density. The use of dilute agarose has a very small effect on the relaxation times of NE. Images were acquired at 9.4 T using ParaVision 6 software (Bruker). Data were acquired using a standard gradient echo method with the following parameters: echo time TE = 0.858 ms, flip angle 52.7°, field of view 9.5 × 9.5 mm, matrix 40 × 40, slice thickness 2 mm and 4 slices. Two sets of images were acquired where TR values were set to one-half of the T_1 values of PFCE and PFCE-Fe-PFHA ([Fe-PFHA] = 30 mM in PFCE oil) nanoemulsions, and the number of averages for each acquisition was adjusted so that the total acquisition time was the same. T_1 of the samples were measured using the spin–echo saturation-recovery method with TR = 70, 100, 200, 300, 400, 6000, 1000, 2000, and 4000 ms, and TE = 6.14 ms. T_2* was measured using a multiple gradient echo method with TE = 1.27, 2.06, 2.85, 3.64, 4.43, 5.23, 6.02, 6.81, 7.60, and 8.37 ms, with TR = 300 ms and flip angle 20°. T_1 and T_2* values were calculated using the ParaVision software.

2.5. Synthesis of Fe-PFHA.

To a stirred solution of PFHA (4.8 mmol, 1.94 g) and sodium acetate (4.8 mmol, 0.394 g) in ethanol (10 mL) was added an aqueous solution of $FeCl_3$ (1.6 mmol, 0.260 g in 10 mL

H_2O). A dark reddish layer was formed immediately at the bottom. The resulting mixture was further heated at 60 °C for 1 h while stirring, cooled to room temperature, and then 0 °C. The solvents were carefully decanted, and the red residual was washed five times with hot water/ethanol (5 mL/5 mL, 60 °C) to remove residual starting materials. The red oil obtained was dried under vacuum pump and turned into red powder after 24 h with a yield of 89%. The product was used directly without further purification. To obtain Fe-PFHA suitable for X-ray crystallography, an oversaturated solution of Fe-PFHA was prepared in hot methanol and stored at 0 °C overnight. The red precipitates were collected by filtration and dried under a vacuum.

2.6. Preparation of Nanoemulsions.

Emulsification was used to formulate PFCE, perfluoropolyether (PFPE), perfluorotetraglyme (PFTG), and perfluoropolyether diethylamide (PFPE-DA) NEs, each containing 20 mM Fe-PFHA. Compound Fe-PFHA (25.3 mg, 0.02 mmol) was added to PFCs (1 mL) and fully dissolved by vortex and bath sonication. An aqueous solution of Pluronic F68 (1.43 mL, 0.1 g/mL) was added. The mixture was vortexed at high for 2 min, followed by addition of 3.57 mL of purified water. The final mixture was vortexed at high for 2 min, followed by probe ultrasonication for 2 min (Omni Ruptor 250 W, 30% power, Omni International, Tusla, OK). The orange colored pre-emulsion was passed five times through a microfluidizer (LV1, Microfluidics, Newton, MA) operating at 20 000 psi and filtered through a 0.8/0.2 μm Supor membrane (#4187, Pall, Port Washington, NY) into sterile glass vials. The vials were sealed and stored at 4 °C. Also, PFCE NE containing Fe-free PFHA (60 mM) was prepared in the same manner as above by mixing PFHA (24.24 mg, 14.8 μL) with 1 mL of PFCE. For PFOB NE emulsification, a lipid film was produced by dissolving 160 mg of lecithin, 32 mg of cholesterol and 3 mg of 1,2-dipalmitoyl-*sn*-glycero-3-phosphoethanolamine (16:0 PE, Avanti Polar Lipids, Alabaster, AL) in chloroform, followed by slow evaporation while rotating, and then drying under high vacuum for 2 days. Compound Fe-PFHA (25.3 mg, 0.02 mmol) was added to PFOB (1 mL) and was fully dissolved by vortex and bath sonication. The lipid form prepared was hydrated with 5.0 mL of purified water by probe ultrasonication for 2 min and then added to the PFOB solution. The final mixture was vortexed at high for 2 min, followed by probe ultrasonication and emulsification using the same methods above. For ^{19}F NMR relaxivity measurements of Fe-PFHA, NEs containing different concentrations of Fe-PFHA (5–30 mM) in PFCs (1 mL) were also prepared using the same methods.

2.7. Cytotoxicity and Cell Uptake.

The murine macrophage cell line RAW264.7 (TIB-71, ATCC, Manassas, VA) was maintained in Dulbecco's modified eagle media containing 10% fetal bovine serum (FBS), 10 mM 4-(2-hydroxyethyl)-1-piperazineethanesulfonic acid (HEPES), 1 mM sodium pyruvate, and 1.5 g/L sodium bicarbonate at 37 °C in 5% CO_2 atmosphere. Cells (3×10^6) were grown in 10 cm^2 cell culture dishes. PFCE NEs containing 20 mM Fe-PFHA or 60 mM PFHA were added at a fluorine concentration of 2.5–10 mg/mL, which was confirmed by ^{19}F NMR. Final volumes of the culture media were adjusted to 5 mL. After incubation overnight at 37 °C, cells were washed three times in phosphate-buffered saline (PBS) to remove free NE and resuspended in 1 mL of PBS. Ten microliters of the cell suspension was

mixed with 10 μL of 0.4% Trypan blue stain, which was then loaded to the glass slide of the cell counting instrument (Countess II FL Automated Cell Counter, Fisher Scientific) to measure viable and nonviable cell numbers following the vendor's instructions. Cell pellets were prepared by centrifuge (×1000, 4 min) to remove liquid, and cells were lysed immediately by adding 100 μL of lysis buffer (above). The mixture was pipetted up and down several times to homogenize suspension. The suspension was transferred to a 5 mm NMR tube, followed by the addition of 100 μL of D_2O/H_2O (1/9) containing 10 mM NaTFA. The ^{19}F uptake was calculated based on the integrated fluorine NMR signals and the number of counted cells.

3. RESULTS AND DISCUSSION

The Fe-PFHA chelate synthesis scheme is displayed in Figure 1. Fe-PFHA was precipitated out as viscous red oil when an aqueous solution of ferric chloride was titrated into an ethanolic solution of PFHA (Figure 1). With a simple wash-and-dry step, Fe-PFHA was obtained in multigram scales in high purity, as confirmed by elemental analysis, including inductively coupled plasma mass spectrometry (ICP-MS), as well as halide and CHN elemental analyses (Table S1).

The X-ray structure of Fe-PFHA reveals a slightly twisted octahedral structure, with an averaged Fe–O bond length of 1.993 Å and an averaged O–Fe–O angle of 174.7° (Figure 2). Interestingly, only the meridional isomer of Fe-PFHA is observed instead of the facial one, which is possibly due to the strong affinity between two adjacent fluorous chains.

We tested the solubility of Fe-PFHA in various PFCs that are commonly used in ^{19}F MRI studies (Table 1). Among them, the highest solubility was observed in PFOB, followed by PFCE and PFTG. In addition, Fe-PFHA displays notably high solubility in very nonpolar perfluorohexanes (PFH, 755 mM) and perfluoromethylcyclohexane (PFMC, 1155 mM). Overall, we speculate that Fe-PFHA should be soluble in most fluorous solvents.

We next examined the efficiency of Fe-PFHA as a ^{19}F T_1 accelerator in a panel of prepared NEs. In brief, Fe-PFHA was fully dissolved in PFC and then emulsified with surfactant (Pluronic F68 or lecithin) via the process of vortexing, sonication, and microfluidization (see Section 2.6). Resulting NEs display a milky orange appearance with a mean particle size of 140–180 nm with polydispersity index (PDI) < 0.1 indicating a uniform particle distribution (Figure 3). As shown in Table 1, Fe-PFHA sharply reduces relaxation times of all prepared NE. Addition of 20 mM Fe-PFHA (~1.8% weight percentage of PFC) is adequate to reduce ^{19}F T_1 and T_2 significantly at 9.4 T. The ferric chelate increases the relaxation rate of fluorine atoms through paramagnetic relaxation enhancement (PRE) effect, which arises from the fluctuating magnetic dipolar interaction between the fluorine nucleus and the unpaired electrons of the iron center.[25] The PRE effect is inversely proportional to the sixth-power of iron–fluorine distance. In the case where the ferric chelate is covalently bound to fluorine atoms, the intramolecular PRE effect is substantially stronger, and the T_1 and T_2 reduction are even more significant, as evidenced by the severe line-broadening observed in the ^{19}F NMR spectrum of Fe-PFHA compound (Figure S2). In NE, the largest longitudinal relaxivity (r_1) for ^{19}F is observed in PFOB, while the largest transverse relaxivity (r_2) for ^{19}F

is observed in PFPE-DA. Ideally, to boost the sensitivity of spin-density weighted ^{19}F MRI, the agent should exhibit high r_1 relaxivity and low r_2 relaxivity. The highest r_1/r_2 ratio for ^{19}F is observed with PFOB (0.647), followed by PFTG (0.435) and PFCE (0.362). Compared with the previously reported r_1/r_2 = 0.191 for FETRIS[25] in PFPE, and r_1/r_2 = 0.467 for SALTAME[26] in PFOB, Fe-PFHA is more efficient and requires less iron complex to achieve comparable T_1 reduction. The difference in relaxation rates observed in various perfluorocarbons is likely to originate from their different molecular weights and viscosity, which affects the rotational correlation time of fluorine atoms.[25]

The long-term stability of NEs containing either 20 mM Fe-PFHA (Fe:PFHA = 1:3) or Fe-free PFHA (60 mM) were tracked over 200 days (Figure 3) and particle size remained stable in the range of 140–180 nm with PDI < 0.1 during this period; a modest size increase in the first 2 weeks is typical behavior for formed NEs. After 250 days, the particle size exceeded 200 nm, but no visible aggregated oil droplets were observed. Additionally, a higher concentration of Fe-PFHA (30 mM) does not appear to affect NE stability (Table S5).

To assess the iron binding stability of Fe-PFHA, both as free chelate and encapsulated in NE droplets, we performed ethylenediaminetetraacetic acid (EDTA) chelate competition experiments. Not surprisingly, in solution Fe-PFHA (0.1 mM in CF_3CH_2OH/H_2O) dissociates quickly, within 30 min, upon the addition of an equal amount of EDTA, with an estimated dissociation constant of 1.68×10^{-6} M^2 (Figure S6). In contrast, for chelate in NE, where EDTA only has very limited access to Fe-PFHA on the outer surface of NE, the competition reaction is presumably diffusion restricted and has a much slower rate (Figure S8). For example, the loss of Fe from Fe-PFHA in NE (measured by absorbance at 438 nm) is only 4.8% after 24 h following treatment with a large excess of EDTA (10 mM in bulk solution). Under the same conditions, we followed the change of relaxation time of NE long-term (Figure 3). The T_1 increased by 31% at week 1 and 88% at week 4, corresponding to a calculated iron loss of 32 and 56% from Fe-PFHA to form Fe-EDTA. However, cell tracking experiments using ^{19}F MRI are usually complete within a week after agent administration. Moreover, the hexadentate EDTA in high concentration is a strong iron chelator and Fe-EDTA (log K_f = 25.1) has higher stability than Fe-transferrin (log K_f = 20.7),[27] a representative protein chelate (pH 7.4). Thus, the potential dissociation and leakage of Fe-PFHA from NE is of minor concern for further cell and in vivo studies.

For in vivo imaging experiments, the total amount of Fe delivered with intravenous injection of Fe-PFHA NE would be very small. For example, in mouse inflammation experiments, often 0.2 mL of NE (~150 mg F atoms/mL) is administered intravenously,[26] corresponding to ~37 μg Fe (assuming [Fe] = 20 mM in PFCE oil); a small fraction of this Fe could theoretically be released to the organism. However, compared with the total amount of Fe contained in mouse tissues (e.g., ~750 μg Fe in blood pool), any release should not impact iron metabolism. The same scaling argument would apply to mammalian species of larger body weights, where the dose of iron-containing NE would scale commensurately.

In vitro cell studies using PFCE NE with dissolved Fe-PFHA or Fe-free PFHA demonstrate cell biocompatibility as shown in Figure 4. In a phagocytic macrophage cell line (RAW 264.7) labeled with agents by coincubation at 37 °C, both NEs display <10% cytotoxicity

even at high doses in culture (10 mg/mL of fluorine atoms in media) as measured by the trypan blue assay and direct cell counts. In terms of absolute cellular uptake, measured by ^{19}F NMR of labeled cell pellets, both NEs demonstrate comparable mean uptake levels of ~1×10^{12} ^{19}F/cell (incubated at 2.5–10 mg/mL fluorine atoms in media) to the control NE without PFHA. This ^{19}F uptake level is comparable to the value previously reported using PFOB NE in the same cells.[26] In the Supporting Information, we also describe longitudinal stability of Fe-PFHA NE in tissue culture media via DLS (Figure S9), ^{19}F relaxation times in labeled RAW cells (Figure S10), and the MTT cytotoxicity assay (Figure S11).

To demonstrate the feasibility of ^{19}F MRI SNR enhancement, we conducted phantom studies in NE samples with or without Fe-PFHA (30 mM in PFCE) at 9.4 T magnetic field strength. Figure 5 shows that the observed SNR for Fe-PFHA NE was increased by 2.6 fold when each NE sample was imaged with optimal parameters, for the same imaging time, and using a conventional gradient-echo imaging sequence. This SNR increase is close to MRI signal modeling predictions[26] of ~2.5, calculated using the measured ^{19}F relaxation times for each sample. More sophisticated MRI pulse sequences known in the art, such as ultrashort time to echo (UTE),[28,29] will predictably yield greater SNR enhancements, particularly when higher [Fe-PFHA] is added; an explicit comparison of Fe-PFHA NE using optimized pulse sequences is beyond the discussion of the manuscript.

It has been established that β-diketonate molecules, including fluorinated ones, are capable of binding other transition metals in addition to Fe(III).[30–32] We confirm this binding ability of PFHA in PFCE NE with a panel of transition metals using quantitative ^{19}F r_1 and r_2 relaxivity measurements at 9.4 T (Figure 6). When Fe^{3+} was titrated to formed NE at fixed [PFHA], the ^{19}F T_1 relaxation rate reaches a plateau at 0.3 equiv. of Fe^{3+} added (Figure S11), consistent with a 1:3 ratio of Fe^{3+} coordination to PFHA as observed in the X-ray structure. Noteworthy, unbound, or excess metals in aqueous phase have no major effects on the relaxation of fluorine atoms as they are in different phases (Figure 6). Additionally, for other metals tested, the relaxation rates reach a plateau when 0.2–0.4 equiv. of metals are added, indictive of a 2–5 coordination number of metals to PFHA (Figure S11). In brief, the bivalent metals give a coordination number of two, whereas lanthanide metals display a coordination number of 4 or 5. Thus, the fluorinated PFHA can act as a versatile chelator for different metals.

As shown in Figure 6 (see also Table S6 and Figure S12), Fe(III) yields the highest r_1 (0.42 s^{-1} mM^{-1}) with a relatively low r_2 (1.31 s^{-1} mM^{-1}) for ^{19}F in NE. The largest r_1/r_2 ratio for ^{19}F was observed using Ni(II); however, the overall low r_1 and r_2 values make it inefficient, and a high dose of Ni-PFHA would be required. For ^{1}H MRI, Mn(II) is a potent contrast agent with a relatively high magnetic moment, however, Mn-PFHA is inefficient for ^{19}F MRI with a r_1 value of 0.067 s^{-1} mM^{-1}. We speculate that Mn(II)-PFHA is not aerobically stable and is rapidly oxidized to Mn(III) or Mn(IV) that have low magnetic moments. This process may be further facilitated by the high solubility of oxygen in PFC. The lanthanide ions, including Gd(III), show very large r_2 (3.35 s^{-1} mM^{-1}) and small r_1 (0.26 s^{-1} mM^{-1}) relaxivities (Figure 6), rendering these ions less useful than Fe(III) for SNR enhancement.

As lanthanide ions are commonly used as solvent NMR shift reagents,[33] we also examined the ^{19}F chemical shift of PFCE NE containing lanthanide-PFHA (Figure S13). Among all the ions tested, Ho(III)-PFHA and Dy(III)-PFHA (30 mM) in PFCE NE induced significant shifts of approximately −0.5 ppm. This observation is consistent with previous studies showing that Ho and Dy, which have large Bleaney coefficients, are able to induce strong pseudocontact shifts as defined by the McConnell–Robertson equation.[34]

When Fe(II) was used instead of Fe(III) as the iron source, the Fe(II)-PFHA complex was formed instantaneously, as evidenced by the immediate drop in ^{19}F relaxation times of PFCE (Figure 7). Formation of Fe(II)-PFHA complex is potentially confounded by an aerobic oxidation of Fe(II) to Fe(III) in situ (Figure 7). A preliminary study was performed using Fe(II)-PFHA in PFCE NE for ^{19}F-sensing of hydrogen peroxide, an oxidizer, whose overabundance has been related to a number of pathological conditions.[35,36] To NE formulated with PFHA ([^{19}F] = 155.5 mg/mL), hydrogen peroxide (0.16 mM) was added 10 min after the addition of $FeCl_2$ (0.16 mM). Upon addition of H_2O_2, the T_1 and T_2 of NE were both reduced by 65% to 131 and 52 ms, respectively, which is on the same order as the relaxation times of PFCE expected if Fe(III)-PFHA is used (T_1 = 112 ms, T_2 = 46 ms, 20 mM Fe added in PFCE, Table 1). We speculate that doping NE with PFHA complexed to redox-active metals (i.e., Fe^{2+}, Cu^{1+}, Eu^{2+}) may potentially be useful as a responsive imaging probe for oxidation stress caused, for example, by the Fenton reaction or aerobic oxidation due to hypoxia. For ^{19}F MRI hydrogen peroxide sensing probes, aerobically more stable ferrous complexes featuring higher redox potentials are desirable for future studies.

4. CONCLUSION

We report the characterization and formulation of fluorinated β-diketonate PFHA and its metal complexes. The use of PFHA has been described previously for a handful of synthetic procedures,[37–40] but its use as a potential imaging agent has not been explored. The Fe-PFHA complex has several advantages over previously reported iron complexes for ^{19}F MRI;[25,26] it is readily prepared at multigram scales using a single synthetic step, and it has a single, well-defined structure. We show versatility of PFHA; it is effective in binding a range of transition and lanthanide ions. The Fe-PFHA complex displays favorable solubility in a wide range of PFCs, and is highly effective in accelerating ^{19}F relaxation rates, especially T_1, using a relatively small amount of Fe-PFHA. More generally, PFHA is valuable as it can functionalize PFC, whose chemical modification remains challenging. For example, by utilizing metals with radioactivity or luminescent properties, one could formulate multimodal ^{19}F MRI, PET and/or fluorescence NE-based imaging probes. Additionally, the Fe(II)-PFHA complexes may be useful for targeted sensing of oxidation stress and hypoxia in vivo. Preliminary cytotoxicity measurements of Fe-PFHA NE appear promising, and in vivo imaging studies using the probe are the subject of future investigations. Overall, PFHA metal complexes provide an avenue for improving the sensitivity of ^{19}F MRI, as well as expanding the toolbox for cellular-molecular imaging applications.

Supplementary Material

Refer to Web version on PubMed Central for supplementary material.

ACKNOWLEDGMENTS

We thank Dina Hingorani and Benjamin Leach for helpful discussions.

Funding

This work was financially supported by National Institutes of Health (R01-EB017271, R01-EB024015, R01-CA139579) and the California Institute for Regenerative Medicine (LA1-C12-06919).

REFERENCES

(1). Al-Rubeai M; Naciri M Stem Cells and Cell Therapy; Springer Netherlands, 2014; p 189.Bluestone JA Regulatory T-cell therapy: is it ready for the clinic? Nat. Rev. Immunol 2005, 5 (4), 343–349. [PubMed: 15775994]

(2). Marban E. A mechanistic roadmap for the clinical application of cardiac cell therapies. Nat. Biomed. Eng 2018, 2 (6), 353–361. [PubMed: 30740264]

(3). Schaffler A; Buchler C Concise review: adipose tissue-derived stromal cells–basic and clinical implications for novel cell-based therapies. Stem Cells 2007, 25 (4), 818–27. [PubMed: 17420225]

(4). Emerich DF; Orive G Cell Therapy: Current Status and Future Directions, 1 ed.; Humana Press, 2017.

(5). Srinivas M; Aarntzen EH; Bulte JW; Oyen WJ; Heerschap A; de Vries IJ; Figdor CG Imaging of cellular therapies. Adv. Drug Delivery Rev 2010, 62 (11), 1080–93.

(6). Zhang SJ; Wu JC Comparison of imaging techniques for tracking cardiac stem cell therapy. J. Nucl. Med 2007, 48 (12), 1916–9. [PubMed: 18056330]

(7). Bulte JWM; Daldrup-Link HE Clinical tracking of cell transfer and cell transplantation: trials and tribulations. Radiology 2018, 289 (3), 604–615. [PubMed: 30299232]

(8). Kircher MF; Gambhir SS; Grimm J Noninvasive cell-tracking methods. Nat. Rev. Clin. Oncol 2011, 8 (11), 677–688. [PubMed: 21946842]

(9). Progatzky F; Dallman MJ; Lo Celso C From seeing to believing: labelling strategies for in vivo cell-tracking experiments. Interface Focus 2013, 3 (3), 1–14.

(10). Kim MH; Woo SK; Kim KI; Lee TS; Kim CW; Kang JH; Kim BI; Lim SM; Lee KC; Lee YJ Simple methods for tracking stem cells with (64)Cu-labeled DOTA-hexadecyl-benzoate. ACS Med. Chem. Lett 2015, 6 (5), 528–530. [PubMed: 26005527]

(11). Gholamrezanezhad A; Mirpour S; Bagheri M; Mohamadnejad M; Alimoghaddam K; Abdolahzadeh L; Saghari M; Malekzadeh R In vivo tracking of 111In-oxine labeled mesenchymal stem cells following infusion in patients with advanced cirrhosis. Nucl. Med. Biol 2011, 38 (7), 961–967. [PubMed: 21810549]

(12). Bulte JWM In vivo MRI cell tracking: clinical studies. Am. J. Roentgenol 2009, 193 (2), 314–325. [PubMed: 19620426]

(13). Arbab AS; Frank JA Cellular MRI and its role in stem cell therapy. Regener. Med 2008, 3 (2), 199–215.

(14). Hoehn M; Wiedermann D; Justicia C; Ramos-Cabrer P; Kruttwig K; Farr T; Himmelreich U Cell tracking using magnetic resonance imaging. J. Physiol 2007, 584 (Pt 1), 25–30. [PubMed: 17690140]

(15). Ahrens ET; Bulte JW Tracking immune cells in vivo using magnetic resonance imaging. Nat. Rev. Immunol 2013, 13 (10), 755–763. [PubMed: 24013185]

(16). Ahrens ET; Zhong J In vivo MRI cell tracking using perfluorocarbon probes and fluorine-19 detection. NMR Biomed 2013, 26 (7), 860–871. [PubMed: 23606473]

(17). Flogel U; Ahrens ET Fluorine Magnetic Resonance Imaging, 1 ed.; CRC Press, 2016.

(18). Chapelin F; Capitini CM; Ahrens ET Fluorine-19 MRI for detection and quantification of immune cell therapy for cancer. J. Immunother. Cancer 2018, 6, 105. [PubMed: 30305175]

(19). Temme S; Bonner F; Schrader J; Flogel U 19F magnetic resonance imaging of endogenous macrophages in inflammation. WIREs Nanomed. Nanobi 2012, 4 (3), 329–343.

(20). Ruiz-Cabello J; Barnett BP; Bottomley PA; Bulte JWM Fluorine (F-19) MRS and MRI in biomedicine. NMR Biomed 2011, 24 (2), 114–129. [PubMed: 20842758]

(21). Tirotta I; Dichiarante V; Pigliacelli C; Cavallo G; Terraneo G; Bombelli FB; Metrangolo P; Resnati G (19)F magnetic resonance imaging (MRI): from design of materials to clinical applications. Chem. Rev 2015, 115 (2), 1106–1129. [PubMed: 25329814]

(22). Janjic JM; Ahrens ET Fluorine-containing nanoemulsions for MRI cell tracking. WIREs Nanomed. Nanobi 2009, 1 (5), 492–501.

(23). Peterson KL; Srivastava K; Pierre VC Fluorinated paramagnetic complexes: sensitive and responsive probes for magnetic resonance spectroscopy and imaging. Front. Chem 2018, 6, 160. [PubMed: 29876342]

(24). Chalmers KH; De Luca E; Hogg NH; Kenwright AM; Kuprov I; Parker D; Botta M; Wilson JI; Blamire AM Design principles and theory of paramagnetic fluorine-labelled lanthanide complexes as probes for (19)F magnetic resonance: a proof-of-concept study. Chemistry 2010, 16 (1), 134–48. [PubMed: 19957317]

(25). Kislukhin AA; Xu H; Adams SR; Narsinh KH; Tsien RY; Ahrens ET Paramagnetic fluorinated nanoemulsions for sensitive cellular fluorine-19 magnetic resonance imaging. Nat. Mater 2016, 15 (6), 662–668. [PubMed: 26974409]

(26). Jahromi AH; Wang C; Adams SR; Zhu W; Narsinh K; Xu H; Gray DL; Tsien RY; Ahrens ET Fluorous-soluble metal chelate for sensitive fluorine-19 magnetic resonance imaging nanoemulsion probes. ACS Nano 2019, 13 (1), 143–151. [PubMed: 30525446]

(27). Aisen P; Leibman A; Zweier J Stoichiometric and site characteristics of the binding of iron to human transferrin. J. Biol. Chem 1978, 253 (6), 1930–1937. [PubMed: 204636]

(28). Goette MJ; Keupp J; Rahmer J; Lanza GM; Wickline SA; Caruthers SD Balanced UTE-SSFP for F-19 MR imaging of complex spectra. Magn. Reson. Med 2015, 74 (2), 537–543. [PubMed: 25163853]

(29). Schmid F; Holtke C; Parker D; Faber C Boosting F-19 MRI-SNR efficient detection of paramagnetic contrast agents using ultrafast sequences. Magn. Reson. Med 2013, 69 (4), 1056–1062. [PubMed: 22628001]

(30). Joshi KC; Pathak VN Metal-chelates of fluorinated 1,3-diketones and related compounds. Coord. Chem. Rev 1977, 22, 37–122.

(31). Toscano PJ; Dettelbacher C; Waechter J; Pavri NP; Hunt DH; Eisenbraun ET; Zheng B; Kaloyeros AE Synthesis and characterization of polyfluorinated beta-diketonate transition metal complexes. J. Coord. Chem 1996, 38 (4), 319–335.

(32). Silva WE; Freire Belian M; Freire RO; de Sa GF; Alves S Jr. New homotrinuclear lanthanide complexes: synthesis, characterization and spectroscopic study. J. Phys. Chem. A 2010, 114 (37), 10066–10075. [PubMed: 20738128]

(33). Cockerill AF; Davies GLO; Harden RC; Rackham DM Lanthanide shift reagents for nuclear magnetic resonance spectroscopy. Chem. Rev 1973, 73 (6), 553–588.

(34). Harvey P; Kuprov I; Parker D Lanthanide complexes as paramagnetic probes for 19F Magnetic Resonance. Eur. J. Inorg. Chem 2012, 2012 (12), 2015–2022.

(35). Barnham KJ; Masters CL; Bush AI Neurodegenerative diseases and oxidative stress. Nat. Rev. Drug Discovery 2004, 3 (3), 205–214. [PubMed: 15031734]

(36). Dhalla NS; Temsah RM; Netticadan T Role of oxidative stress in cardiovascular diseases. J. Hypertens 2000, 18 (6), 655–673. [PubMed: 10872549]

(37). Buttner S; Lubbe M; Reinke H; Fischer C; Langer P Regioselective synthesis of 4-alkyl- and 4-aryl-6-(perfluoroalkyl)-salicylic acid derivatives by formal [3 + 3] cyclocondensation of 1,3-bis(silyloxy)-1,3-butadienes with 3-silyloxy-1-(perfluoroalkyl)prop-2-en-1-ones. Tetrahedron 2008, 64 (34), 7968–7976.

(38). Kurykin MA; Volpin IM; German LS Reactions of perfluoroalkylacetones with nucleophilic reagents. J. Fluorine Chem 1996, 80 (1), 9–12.

(39). Nikonov MV; Chizhov DL; Ratner VG; Pashkevich KI Synthesis of polyfluoroalkyl-containing 1,3,5-triketones. J. Fluorine Chem 2000, 106, 115–116.

(40). Popova LM; Ginak AI Cyclocondensation of unsymmetrical perfluoroalkyl-substituted beta-diketones with urea, thiourea, and guanidine. Russ. J. Org. Chem 2008, 44 (4), 489–494.

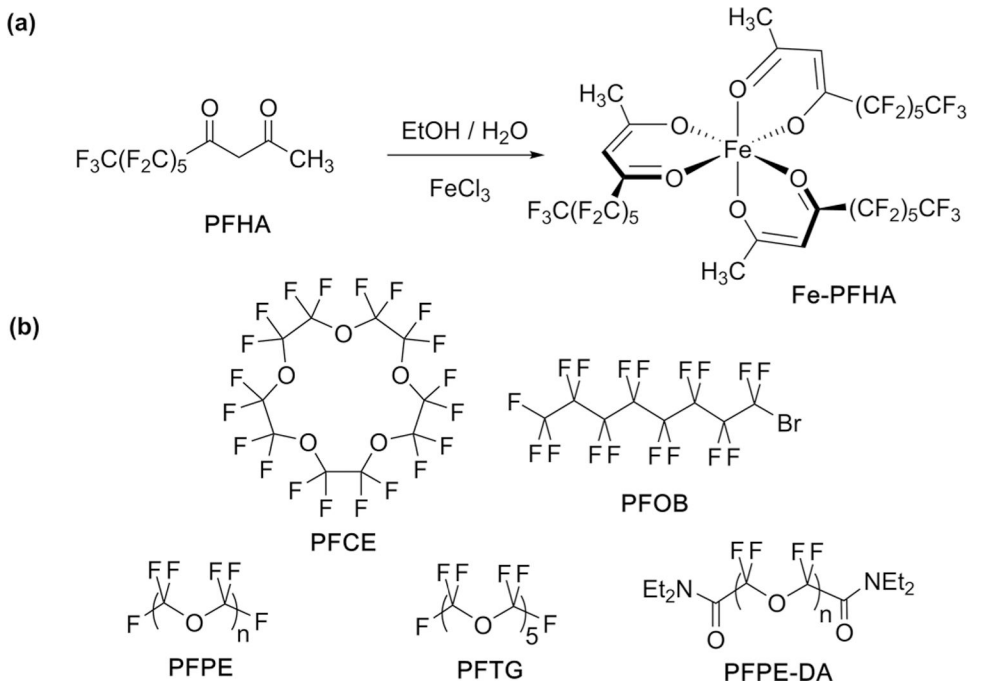

Figure 1.

(a) Preparation of Fe-PFHA from β-diketonate PFHA, and (b) structures of perfluorocarbons used for ^{19}F MRI.

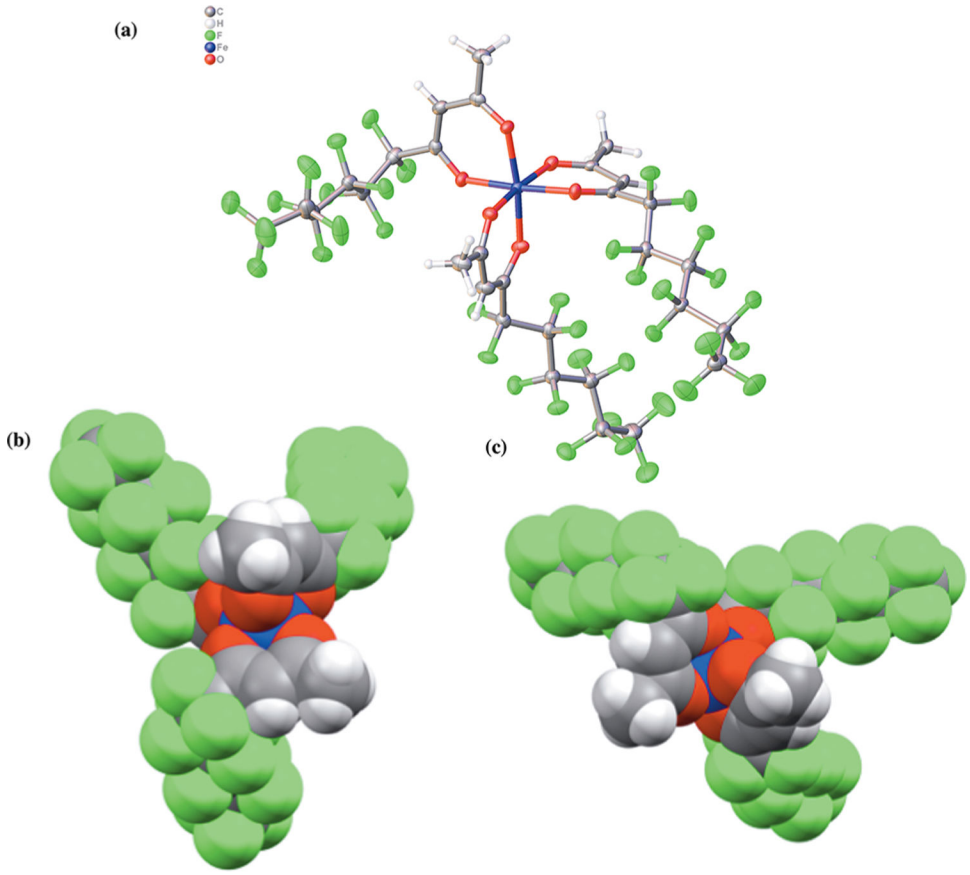

Figure 2.

Crystal structure of Fe-PFHA. (a) X-ray structure, (b, c) space-filling model from (b) top and (c) side views; only one of the two molecules in the unit cell is shown. Color code is gray for carbon, white for hydrogen, green for fluorine, purple for iron, and red for oxygen.

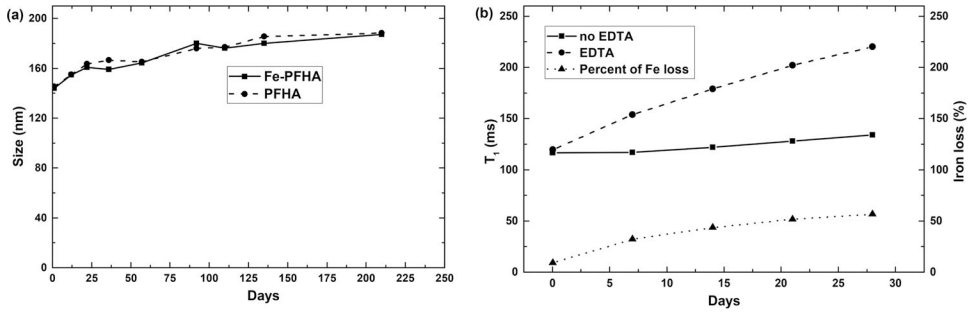

Figure 3.

Temporal stability of formed NE. (a) Particle size of PFCE NE containing 20 mM Fe-PFHA or Fe-free PFHA (60 mM) stored at 4 °C. (b) ^{19}F T_1 relaxation time of PFCE NE (20 mM Fe-PFHA) treated with 10 mM EDTA in PBS buffer (H_2O/D_2O = 9/1) at pH 7.4 over 4 weeks at 4 °C; the effective percent loss of iron from Fe-PFHA to EDTA is calculated and plotted (right ordinate).

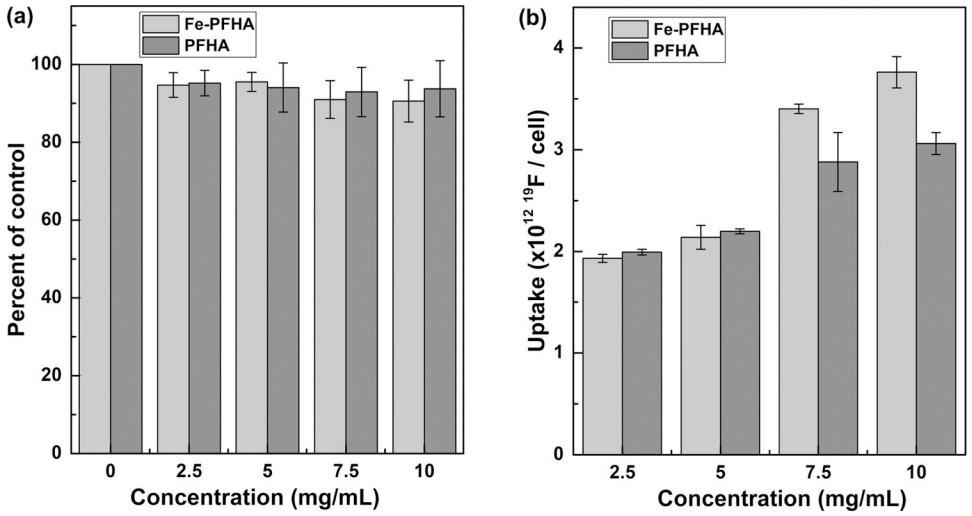

Figure 4.

Viability and cell uptake of RAW cells incubated with PFCE NE. (a) Viability data when cells are incubated with 0–10 mg/mL of NE containing 20 mM Fe-PFHA or Fe-free PFHA (60 mM) for 16 h. (b ^{19}F uptake under the same conditions. Three independent experiments were performed and the standard errors $\left(\mathrm{SD}/\sqrt{N}\right)$ were used as error bars, where $N = 3$.

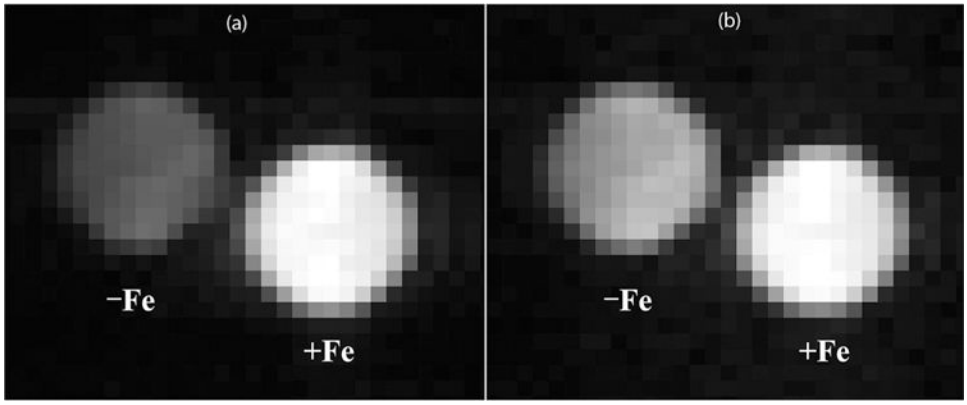

Figure 5.

Phantom ^{19}F images (9.4 T) for PFCE NE with or without iron. (a, b) Nanoemulsion tubes, with MRI scan parameters optimized separately to maximize SNR of PFCE ([Fe-PFHA] = 30 mM in oil) and PFCE (no iron), respectively. Scanning parameters were TR = 37.7 ms and number of averages (NA) = 52 for (a), and TR = 489.5 ms and NA = 4 for (b). Acquisition time was 16 min for both images.

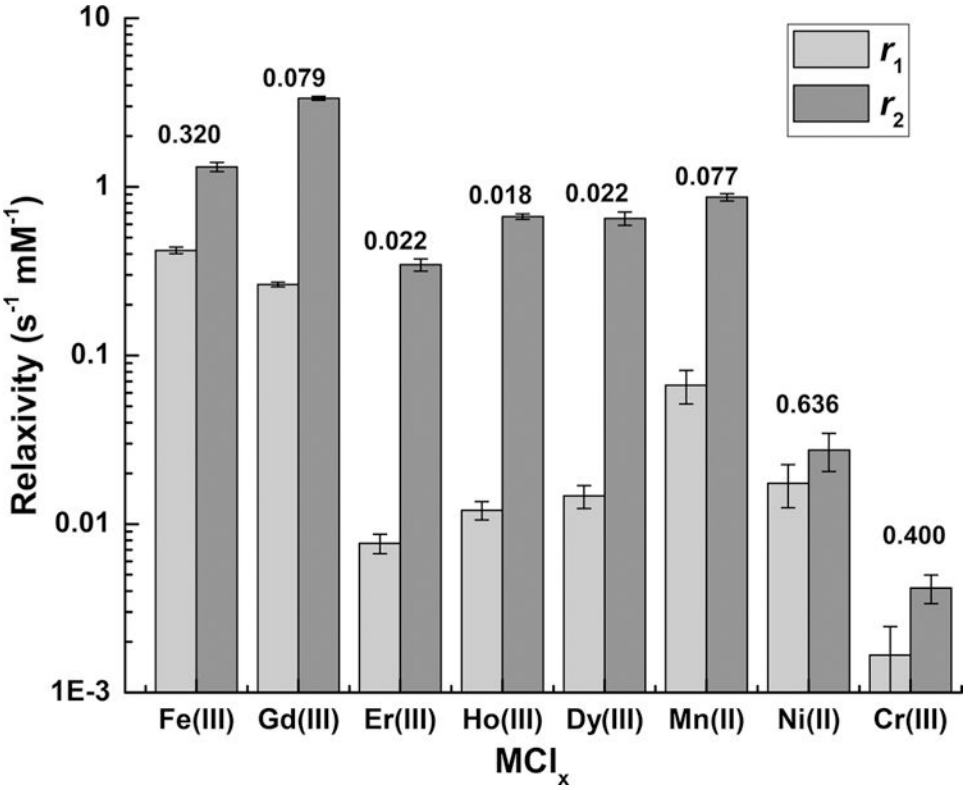

Figure 6.

^{19}F relaxivity of different metal ions in PFHA PFCE NE. The numbers shown at top of bars are the corresponding r_1/r_2 ratios. Note, ordinate is logarithmic scale.

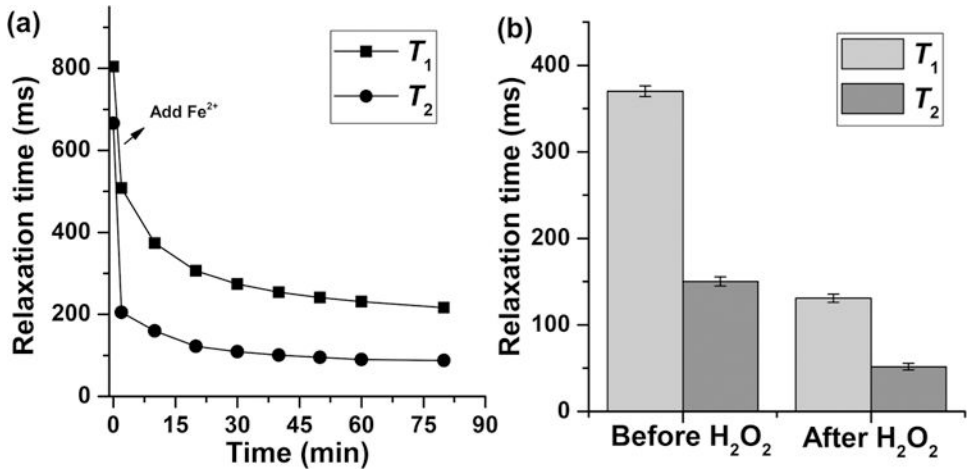

Figure 7.

Use of PFCE NE containing PFHA for sensing H_2O_2. (a) ^{19}F relaxation times of NE upon addition of ferrous chloride. (b) ^{19}F relaxation times when H_2O_2 is added 10 min after adding ferrous chloride. The mixture concentrations are [PFHA] = 0.48 mM, [$FeCl_2$] = 0.16 mM, and [H_2O_2] = 0.16 mM. Three independent tests were performed and the standard errors $\left(\mathrm{SD}/\sqrt{N}\right)$ were used as error bars.

Table 1.

Effect of Fe-PFHA on the Relaxation Times of Various PFC NEs at 9.4 T

		T_1 (ms)		T_2 (ms)				
	solubility (mM)	**no Fe**	**20 mM Fe**	**no Fe**	**20 mM Fe**	**r_1 relaxivity (s^{-1} mM^{-1})**	**r_2 relaxivity (s^{-1} mM^{-1})**	**r_1/r_2**
PFCE	302	804.5 ± 29.8	112.0 ± 3.5	717.2 ± 23.7	45.6 ± 2.2	0.396 ± 0.012	1.093 ± 0.081	0.362
PFOB	672	919.2 ± 26.7	46.5 ± 1.2	839.6 ± 19.3	33.7 ± 1.4	1.012 ± 0.013	1.563 ± 0.046	0.647
PFPE	37	429.2 ± 7.3	103.0 ± 2.0	241.0 ± 6.7	32.9 ± 1.2	0.369 ± 0.029	1.313 ± 0.074	0.281
PFPE-DA	241	401.1 ± 18.0	48.2 ± 1.7	83.0 ± 1.0	10.3 ± 0.5	0.993 ± 0.174	4.858 ± 1.070	0.214
PFTG	114	838.9 ± 21.8	131.6 ± 3.7	697.8 ± 20.9	61.9 ± 2.4	0.320 ± 0.016	0.736 ± 0.024	0.435

ACS Appl Bio Mater. Author manuscript; available in PMC 2021 May 11.